# Selective synthesis of nanosized $TiO_2$ by hydrothermal route: Characterization, structure property relation, and photochemical application

K. Madhusudan Reddy, Debanjan Guin, and Sunkara V. Manorama[a)]
*Nanomaterials Laboratory, Indian Institute of Chemical Technology, Hyderabad 500007, India*
A. Ramachandra Reddy
*Department of Physics, National Institute of Technology, Warangal, Andhrapradesh 506004, India*

(Received 9 January 2004; accepted 22 March 2004)

By variation of reaction temperature and time during the hydrothermal synthesis process, $TiO_2$ nanoparticles in anatase, rutile, and mixture of rutile-anatase phases are formed without adding any mineralizer. Differential thermal analysis studies indicate the rutile phase crystallization at a comparatively lower temperature and a low weight loss. The material synthesized by hydrothermal reaction required no post-calcination for the crystallization. Transmission electron microscopy, selected-area diffraction, Brunauer–Emmett–Teller, and x-ray diffreaction studies confirmed the compositions to be anatase and rutile with the particle size ranging from 5 to 25 nm with surface area as high as 260 $m^2/g$ for the anatase and 65 $m^2/g$ for rutile. The prepared nanoparticles exhibited a blue shift of the absorption edge in the ultraviolet-visible spectrum greater than 10 nm. The particles with average size around 5 nm showed two band edges in the absorption spectra attributed to two different particle sizes. Simple photocatalytic reactions were tried to demonstrate the photochemical activity of the synthesized material. The synthesized nanoparticles exhibited an ultraviolet radiation simultaneous photoreduction of Cr(VI) to Cr(III) and oxidation of formic acid into carbon dioxide and water.

## I. INTRODUCTION

Titanium dioxide possesses interesting optical, dielectric, and catalytic properties, which result in industrial applications such as pigments, dye sensitized solar cells, fillers for catalyst supports, and in photocatalysis.[1,2] As a pure component and as a mixture with other oxides, $TiO_2$ has been associated with improved sensitivity to humidity, oxygen,[3] enhanced mechanical property,[4] and catalytic activity,[5] and it has also been used in membrane separations involving chemical reactions.[6] Titania has been known to exist in several polymorphic forms, of which anatase and rutile have been widely studied. Rutile is the only stable phase, whereas anatase and brookite are metastable at all temperatures and transform to rutile on heating to temperatures above 700 °C.[7] The rutile phase offers an attractive combination of physical properties which has made it the most widely used white pigment in the worldwide market due to its exceptional light scattering efficiency, high refractive index, hiding power, tinting strength, and chemical inertness.[8,9] However, unlike anatase, it is found that the synthesis of ultrafine rutile particles is much more difficult.[10] All the crystalline forms occur in nature as minerals, whereas methods adopted for the synthesis generally produce anatase at low temperatures.[11,12] The anatase form is preferred for applications as membranes in dye-sensitized solar cells, solar energy conversion.[1] Also, studies by Zhang et al. have shown that mixtures of anatase and rutile are found to be more active than the individual phases.[13]

Recently, the hydrothermal-reduction route has been developed as a mild and effective route to synthesize novel materials. Hydrothermal synthesis has been known as a powerful method for the preparation of high-purity, highly crystalline, ultrafine, and homogeneous powders of various single- and multi-component oxide powders. However, many factors like reaction temperature, time, and medium may influence the crystallization process. The hydrothermal method has been exploited earlier to prepare polymorphs of titania with different morphologies from different precursors.[14–17] This paper presents the controlled synthesis of $TiO_2$ nanoparticles with varied rutile/anatase weight ratios by the hydrothermal method by varying the reaction time and temperature.

[a)]Address all correspondence to this author.
e-mail: manorama@iict.res.in
DOI: 10.1557/JMR.2004.0335

  

The possibility of synthesizing anatase, rutile, or a mixture of both at low temperatures, with or without additives, is an important achievement both from the scientific and technological standpoints and this report precisely deals with one such attempt. The paper also presents structural characterization of synthesized materials using various analytical techniques. To demonstrate the photochemical efficiency of the synthesized titania, a test reaction of converting Cr(VI) to Cr(III) and HCOOH to $CO_2$ and $H_2O$ under ultraviolet (UV) light is described and its activity compared with commercial titania (Aldrich Chemical Co., Milwaukee, WI).

## II. EXPERIMENTAL

Titanium tetrachloride (SD Fine Chemical Co. Ltd., Mumbai, India) was used as the starting material without any further purification. In a typical reaction process 2 ml 0.5 M $TiCl_4$ (50% HCl) was added to 50 ml distilled water, and the mixture was taken in a 70 ml Teflon lined autoclave. The autoclave temperature was increased from 80 to 250 °C and held at that temperature for different time durations ranging from 3 to 70 h under autogenerated pressure. After the reaction the system was allowed to cool. The white precipitate obtained is filtered, washed, sonicated and dried at 80 °C overnight. A blue tinge appeared on the walls of the container, which is a clear indication of scattering by the ultrafine particles. The detailed synthesis conditions and the corresponding physical parameters for the different samples are summarized in Table I.

### Material characterization

Powder x-ray diffraction (XRD) was recorded on a Seimens (Cheshire, UK) D5000 X- ray diffractometer over a 2θ range from 2° to 65° using Cu $K_\alpha$ ($\lambda = 1.5406$ Å). The thermal transformations were studied by differential thermal analysis (DTA) system (Mettler Toledo Star$^e$, Columbus, OH) in air, with a heating rate of 20 °C/min. The specific surface area of samples was measured by nitrogen adsorption using a Brunauer–Emmett–Teller (BET) surface area analyzer (Pulse Chemisorb 2700 Micromeritics, Norcross, GA). Diffused reflectance UV (DRUV) studies were performed on a UV spectrometer (Hitachi 330, Gilberts, IL), with an integrated sphere apparatus having a scan speed of 120 nm/cm, in the percentage reflection mode using a slit width of 2 nm and a response time of 2 s. The samples for the UV-visible absorption spectra were in the form of 1 inch diameter pellets with KBr. The spectra were recorded on a Shimadzu (Duisberg, Germany) 240 UV spectrophotometer. A JEOL (Peabody, MA) JEM – 200 CX transmission electron microscope (TEM) operating at 200 KV was used to record the selected-area diffraction (SAED) and the TEM patterns.

## III. RESULTS AND DISCUSSION

The effects of hydrothermal conditions on the properties and structural characteristics of $TiO_2$ nanoparticles

TABLE I. Synthesis conditions; results from XRD, BET surface area, and diffused reflectance spectroscopy of the nanoparticles of titanium dioxide.

| Code | T (°C) | Time (h) | pH | $F_R$[a] | $F_A$[a] | $SA_{BET}$ | $d_{BET}$ (nm)[b] | $d_{XRD}$ (nm)[c] | Band gap (eV)[d] |
|---|---|---|---|---|---|---|---|---|---|
| A | 80 | 10 | ~5 | ⋯ | 1.00 | 266 | 05.1 | 04.3 | 3.31 |
| B | 150 | 15 | <2 | 0.29 | 0.71 | 112 | 14.7 | 10.6 | ⋯ |
| C | 150 | 45 | <2 | 0.37 | 0.63 | 106 | 15.5 | 11.8 | 3.18 |
| D | 150 | 70 | <2 | 0.45 | 0.55 | 89 | 16.6 | 13.7 | 3.15 |
| E | 170 | 05 | <2 | 0.16 | 0.84 | 166 | 09.8 | 09.3 | 3.27 |
| F | 170 | 12 | <2 | 0.25 | 0.75 | 110 | 14.4 | 10.7 | 3.22 |
| G | 170 | 24 | <2 | 0.30 | 0.70 | 105 | 15.6 | 13.9 | ⋯ |
| H | 170 | 62 | <2 | 0.48 | 0.52 | 72 | 23.8 | 15.7 | 3.18 |
| I | 180 | 12 | <2 | 0.30 | 0.70 | 139 | 11.2 | 08.3 | 3.22 |
| J | 180 | 70 | <2 | 0.70 | 0.30 | 64 | 25.9 | 19.4 | 2.98 |
| K | 190 | 24 | <2 | 0.44 | 0.56 | 95 | 18.2 | 12.9 | 3.11 |
| L | 200 | 03 | <2 | 0.27 | 0.73 | 180 | 08.6 | 04.7 | 3.16 |
| M | 200 | 06 | <2 | 0.33 | 0.67 | 154 | 10.3 | 07.8 | ⋯ |
| N | 200 | 12 | <2 | 0.37 | 0.63 | 106 | 15.5 | 11.6 | 3.19 |
| O | 200 | 24 | <2 | 0.75 | 0.25 | 80 | 18.2 | 15.4 | 2.96 |
| P | 200 | 70 | <2 | 1.00 | ⋯ | 66 | 31.0 | 18.2 | 2.88 |
| Q | 250 | 10 | <2 | 1.00 | ⋯ | 61 | 35.0 | 20.7 | 2.87 |
| R | 120 | 10 | ~8 | ⋯ | 1.00 | 109 | 13.4 | 07.8 | 3.25 |

[a]Fraction of rutile by Spurr equation (Ref. 23).
[b]Particle size by equation (Ref. 28) using BET surface area.
[c]Crystallite size from XRD using Scherrer formula (Ref. 22).
[d]Band-gap energy is estimated from the $(\alpha h\nu)^2$ versus $(h\nu)$ plot, replotted using DRUV spectrum (Ref. 30): A deviation of ±5% is to be considered for the data in the table.

are summarized in Table I. It is observed that titanium dioxide crystallization into anatase phase decreases with the increase of the hydrothermal temperature from 150 to 200 °C. The particle size of the anatase and rutile nanoparticles are found to vary from 10 to 35 nm and with a corresponding specific surface area in the range of 100–200 $m^2/g$. Hydrothermal synthesis is considered to be a hydrolysis reaction accompanied by accelerated dehydroxylation. $TiO_2$ crystallizes into rutile phase at very low temperatures compared to other methods. It is also known that the pH of the medium and the cation has a pronounced effect on the phase composition obtained.[18,19] For a highly acidic solution, rutile phase is formed at low temperatures. This is mainly because in such an acidic medium, with the dissolution of the precursor, the grain growth is more rapid compared to the process in a basic medium. Anatase phase is favorably obtained when the solution pH is around 8. We could obtain the rutile phase at around 200 °C, where the reaction was carried for 70 h, which is at low temperature when compared to a previously report.[10] Thus the formation of rutile phase is justified by the highly acidic media in previous reports.[10,20] The significant result from our present studies is that even without adding any mineralizer, we are able to synthesize rutile phase at conveniently low temperatures. This low-temperature synthetic route, based on simple reactions with no participation of catalysts or templates and requiring no expensive and precise equipment, will ensure high purity in the products and greatly reduce the production cost. The process thus provides an opportunity for easy scaling up operation to obtain nanostructured materials in the required phase. The phase formed is governed by the rate of aggregation of the octahedral complexes. In the presence of acid, the aggregation processes are inhibited due to repulsion from adsorbed $H^+$ ions.[21] The higher the acid concentration is, the higher the repulsion and the slower the aggregation. Hence, rutile phase is formed when the acid concentration is high. At high pH, the repulsion forces are less, promoting faster aggregation and therefore the formation of anatase. Reaction temperature and reaction time also influence the phase of crystallization. In the highly acidic solutions, it is found that the average grain size of the products increases with the prolonged reaction time. Therefore, a series of titania nanoparticles with different phases and with tunable particle size/surface areas is obtained simply by varying the hydrothermal temperature, pH of solution, and reaction time.

### A. XRD and phase quantification

Powder XRD patterns of the as-prepared samples are presented in Figs. 1(a)–1(d). All the x-ray patterns for the hydrothermally synthesized titanium powders were identified as titania in anatase or rutile phase with the

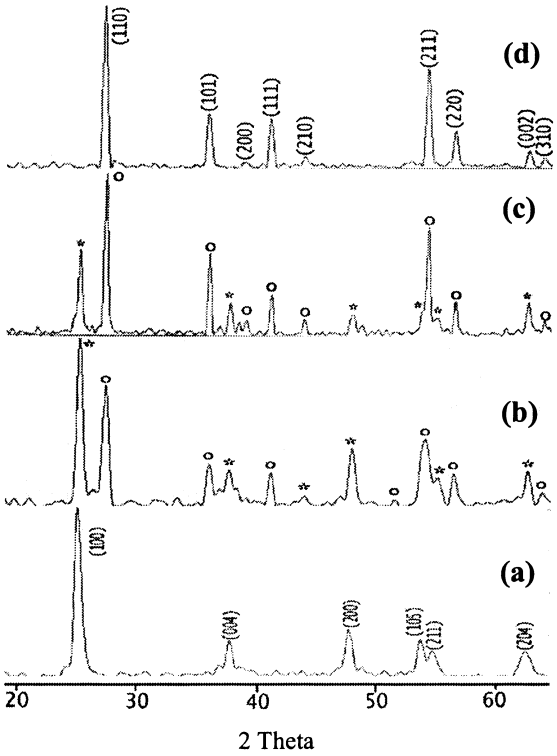


FIG. 1. Powder x-ray diffraction patterns of selected samples prepared at (a) 120 °C for 12 h, (b) 170 °C for 24 h, (c) 200 °C for 24 h, and (d) 250 °C for 10 h. The peaks are labeled for their corresponding planes and (o) denotes the anatase phase while (*) denote the rutile phase.

diffraction peaks narrowing with increasing hydrothermal temperature and the heating duration, indicating increase in the corresponding crystallite sizes. Figure 1(a) gives the pattern for the sample synthesized at 120 °C for 12 h that demonstrates the anatase phase. Figures 1(b) and 1(c) give the patterns with anatase and rutile phases in different proportions synthesized at 170 °C/24 h and 200 °C/24 h. Figure 1(d) is the XRD pattern for the sample at 250 °C/10 h showing the rutile formation. The reflections that correspond to anatase (JCPDS powder diffraction data card no. 21-1272) and rutile (JCPDS powder diffraction data card no. 21-1276) phases were analyzed. The (101) and (110) plane peaks of the anatase and rutile phase were used to calculate the anatase and rutile crystallite sizes, respectively. The average crystallite size is within 5–20 nm determined by applying the Debye–Scherrer formula[22] to the maximum intensity reflection peak. The fraction of rutile phase present in each sample (A through Q) was determined by the usually accepted quantitative method.[23] This method consists of measuring the relative XRD intensities of the anatase [101] ($d$ = 3.520 Å) and the rutile [110] ($d$ = 3.247 Å) peaks. Then, the mass fraction of rutile ($F_R$) was determined from the following Spurr expression: $F_R = 1/[1 + 1.26(I_A/I_R)]$ where $I_A$ and $I_R$ are the integrated line intensities of the anatase and rutile, respectively. These

diffraction lines are used for measuring the fraction of rutile phase, because of the strong intensity and symmetrical shape of the peak. Figure 2 demonstrates the rutile fraction formed for the corresponding reaction temperature, the reaction time being fixed at 12 h. The trend that fewer nanoparticles were crystallizing into the anatase phase suggests that rutile nanoparticles with tunable morphologies/sizes may be prepared by simply adjusting the acidity or reaction temperature and time. From 150 to 180 °C there has not been much increase in the rutile phase and both the phases coexisted. The strong influence of the reaction temperature and the acidity of the medium on the crystallization of the titania was further evident in the synthesis of samples as described in the following sections.

## B. TEM

Figure 3 represents the nanoparticles of titanium dioxide with their corresponding SAED pattern and histograms representing the particle size distribution. It is to be noted that Fig. 3 depicts nearly monodispersed nanoparticles for the sample prepared at 80 °C for 10 h. Average particle size of about 5 nm that increases with the time of the hydrothermal treatment is observed, as seen in Table I. The d-spacings calculated from the SAED patterns agree with those of titania in the anatase phase, which is given in Fig. 3(a) (center). With increase of the reaction temperature (170–200 °C) and time (12–24 h) the crystallite size of anatase phase gradually increases from several nm to approximately 20 nm in the present reaction medium. Particle size increased to nearly 20 nm for the sample prepared at 190 °C and the corresponding SAED diffraction [Fig. 3(a) left and center] has rings that correspond to anatase and rutile forms of titanium dioxide. With further increase in the hydrothermal temperature (~250 °C) and time (10–12 h) for the acidic solution (pH ~ 2) the rutile phase is exclusively formed. It is observed that at temperatures above 200 °C titanium dioxide easily crystallizes into the rutile rather than anatase phase as explained in the earlier section. The histogram shows a peak at about 14 nm. Figure 3(c) shows the rutile crystallites of titania with a particle size around 20–35 nm synthesized at 250 °C. We can observe the characteristic spots in the SAED pattern [Fig. 3(c), center] for these samples normally seen for single crystals instead of the diffraction rings. This is indicative of large crystallites of the rutile titania. This is expected since the dehydroxylation reaction at higher temperatures is faster in hydrothermal reaction, and therefore one can expect these large crystals. Thus the SAED gives a clear idea of the degree of crystallinity that is obtained by the hydrothermal process. Correspondingly the histogram shows a maximum particle size of about 26 nm.

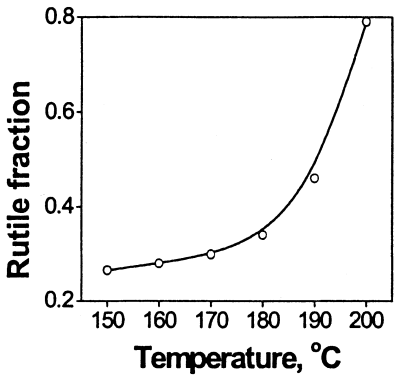


FIG. 2. Plot showing the fraction of rutile formed versus reaction temperature. Reaction time was held for 12 h. Dots represent the calculated points.

## C. DTA

Figure 4 shows the thermogravimetric (TG)/differential thermal analysis (DTA) data of some typical samples that reveal the characteristics temperatures of phase transformation and crystallization. Figure 4(a) shows the DTA curve for the sample synthesized with initial pH 2, and hydrothermally treated at 80 °C for 10 h The sharp endothermic peak at 100 °C corresponds to the loss of water, as well as a possible amorphous material present that crystallizes into anatase phase at 400 °C. DTA curve for sample prepared at pH 8, hydrolyzed with $NH_4OH$, is being presented in Fig. 4(b). Around 450 °C, the material crystallizes into anatase. This was also confirmed by XRD results after calcination at 450 °C. In another set, titania was synthesized from titanium tetrachloride and subjected to hydrothermal treatment. Figure 4(c) is the DTA curve for the sample M. The sample was synthesized from a $TiCl_4$ solution with initial pH 2 by hydrothermal treatment at 200 °C for 6 h. This shows an endothermic peak at 100 °C that is due to water loss and the correponding TG gives a weight loss of approximately 10%. The second broad endothermic peak around 300–400 °C could be due to the formation of anatase form of titania. There is a sharp exothermic peak over this, which could be due to some crystallization of titania directly into the rutile phase. The other endothermic peak at high temperatures approximately 900 °C could be due to the anatase tranformation into rutile. These observations are corroborated in our XRD data and there is approximately 35% rutile fraction by mass and the rest is anatase. Figure 4(d) shows the DTA of sample synthesized by hydrothermal treatment of $TiCl_4$ solution with initial pH 2 at 250 °C for 10 h. This extended hydrothermal treatment results in the formation of direct rutile phase. The as-synthesized material is to a large extent rutile as seen in Fig. 1(d). The amorphous phase also crystallizes into the rutile phase at 200 °C, and this justifies the presence of only rutile phase in the XRD. The small endothermic peak at about 675 °C

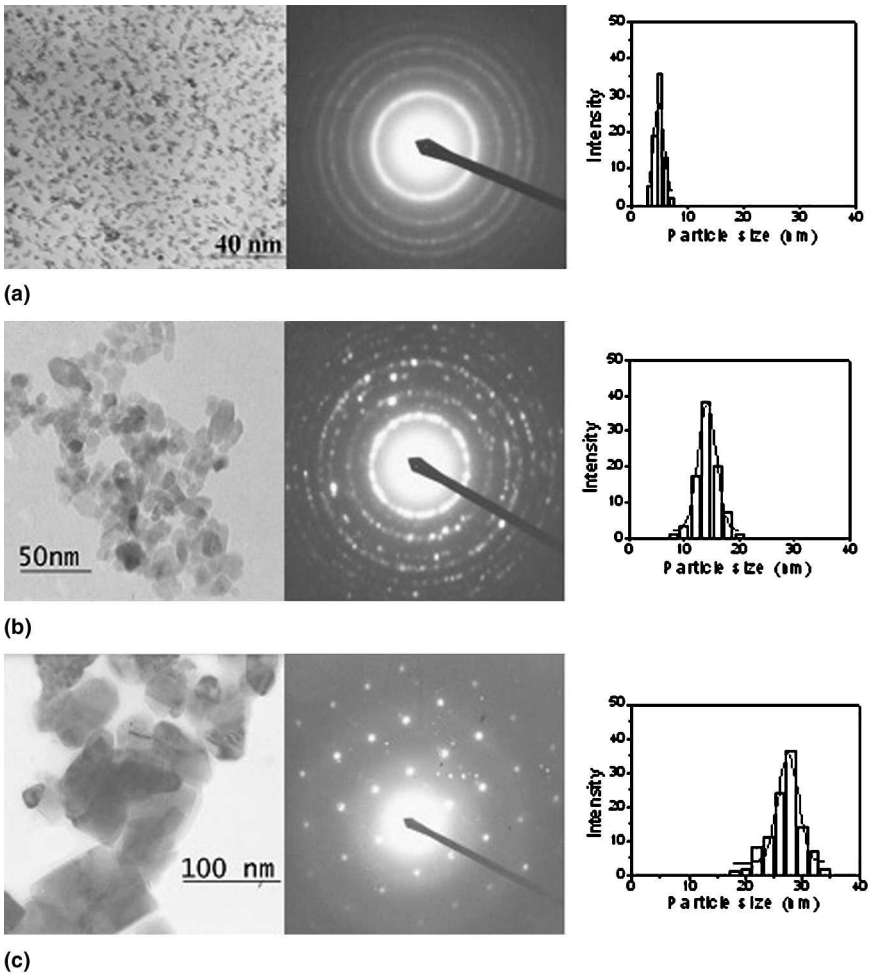


FIG. 3. Typical transmission electron micrograph, selected area electron diffraction and histogram showing the particle size distribution: (a) samples prepared at 80 °C for 10 h, showing the anatase phase; (b) sample prepared at 190 °C for 24 h, showing both anatase and rutile phases; and (c) samples prepared at 250 °C for 10 h, showing the rutile phase.

could be the same 900 °C endothermic shifted to lower temperatures.

### D. BET surface area ($N_2$ adsorption)

Samples were pre-heated at 150 °C under nitrogen flow before the nitrogen adsorption studies were carried out. All the results are presented in Table I. We can observe that increase in crystallite size has an effect over the samples, which gives decrease in the surface area. For 200 °C there is a decrease in the surface area with increase in the reaction time as can be observed in entries from L through P. For the sample prepared at low temperature and lesser time periods for example, at 80 °C for 10 h the surface area value attained a maximum of approximately 260 $m^2/g$, which is quite high compared to the commercially available $TiO_2$ (30–40 $m^2/g$). Surface area as high as 60 $m^2/g$ is observed for rutile titania and even higher values were observed for compounds with mixed phases. The high surface area is an important criterion for applications such as rutile-based titania for dye-sensitized solar cells,[24] solar reflecting shields,[25–26] and gas-sensing catalysis.[27] The reduction in the surface area or the increase of the crystallite size with increased hydrothermal temperature could be attributed to densification, which is associated with a dissolution–precipitation process that improves the crystallization of nanopowders. Particle size is also estimated from the surface area measurements using the following equation[28]

$$d_{XRD} = 6 \times 10^4/(\text{Surface area} \times \text{Density of the sample}).$$

The difference between the average particle size ($d_{BET}$) from BET specific surface area and the crystallite size by XRD ($d_{XRD}$) can probably be ascribed to the significant amount of aggregation that occurs in most of the samples. Table I summarizes all the values obtained.

### E. Diffused reflectance UV spectroscopy

Diffused UV-visible reflectance spectra for the tita nium dioxide samples synthesized at different hydrothermal

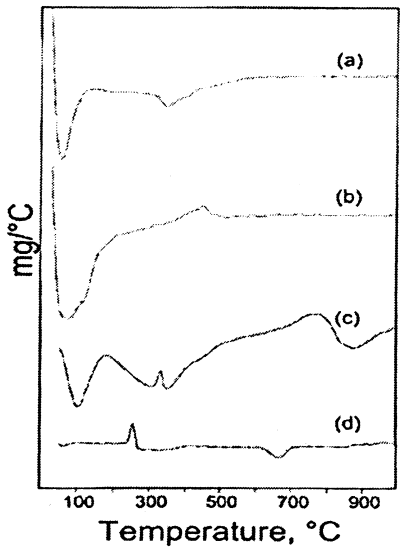


FIG. 4. Differential thermal analysis plots of sample synthesized from $TiCl_4$ solution at pH 2 subjecting to hydrothermal treatment at (a) 80 °C for 10 h, (b) by adding $NH_4OH$ and maintaining pH 8, (c) 200 °C for 6 h, and (d) 250 °C for 10 h.

temperatures are recorded and compared. It is seen that for smaller particles the absorption edge is shifted toward lower wavelength (higher energy), termed as blue shift, which is a characteristic phenomena in nanoparticles. Titanium dioxide particles of 4–5 nm follow the direct band transition behavior, and with the increase in the particle size it tends to follow indirect band transition. With the increase in the particle size, there is almost a 10 nm shift in the absorption edge, the band-gap energy decreases with increasing time and temperature. Band-gap energy is calculated using the equation given in an earlier report.[29] In a previous report by our group, it was shown that nanoparticles of titanium dioxide followed a direct band transition.[30] On plotting for direct band transition behavior using the equation reported earlier[31] and analyzing the graphs, we report the band-gap energy as shown in Table I. However, further experiments have to be carried out to demonstrate whether the shift in absorption edge is purely due to the variation of particle size or is a result of varying compositions of the phases present.

### F. Quantum size effects

To bring out the correlation between the band-gap energies and the grain sizes for the as-prepared titania nanoparticles their UV spectra of the colloidal nanoparticles were recorded. Figure 5 represents the UV absorption spectra and fitted curves of colloidal titanium dioxide obtained after 12 and 18 h of hydrothermal treatment at 80 °C. Interestingly, two pronounced peaks appear at 258 and 304 nm, and these remain unchanged for samples prepared with different reaction time periods in agreement with the results of Yuhong et al.[32] For smaller particle size, the relative content of the peak at shorter wavelength becomes higher. To obtain the band-gap energy of the samples we have plotted ln $\alpha$ versus energy (in eV) in Fig. 6. Urbach's rule[33] suggests to use the values between ln $\alpha = 6$ and ln $\alpha = 10$ for estimating the band-gap of semiconductors. The linear portion of the curves were found between ln $\alpha = 7$ and ln $\alpha = 9$. For the curves in the figure the linear partition of samples prepared at 180 °C/18–12 h is between ln $\alpha = 6.5$ and ln $\alpha = 8.5$ (indicated by arrows in the figure) and the band-gaps are found to be 3.25 and 3.32 eV, respectively. Band-gap energy obtained in this study is very close to band-gap energy of anatase titanium dioxide. Present values indicate that the small particle size results in the band-gap shift of nearly 0.1 to 0.2 eV compared with that of bulk anatase titanium dioxide.

### G. Photocatalytic reaction

A test photochemical reaction to demonstrate the improved photoreactivity of the synthesized titania nanocrystals as described below was carried out. There are reports where titanium dioxide nanopowders were synthesized and applied in photocatalysis. Hirano et al. prepared $TiO_2$ fine powders doped with $ZrO_2$ and applied them to methylene blue photocatalysis.[34] Anatase-Brookite biphase samples were prepared and studied for

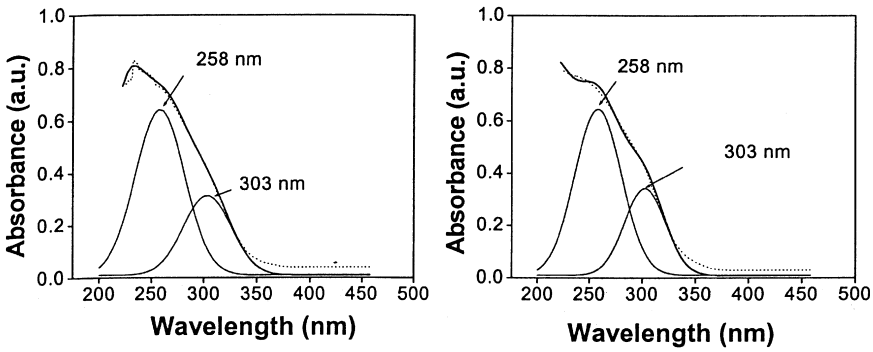


FIG. 5. UV-vis absorption spectra of the nanoparticles of titanium dioxide synthesized at 80 °C for 12 and 18 h. The dotted line represents the curve obtained by the experiment, and the solid line is the fitted curve. Two Gaussian peaks are centered at 258 nm and 303 nm.

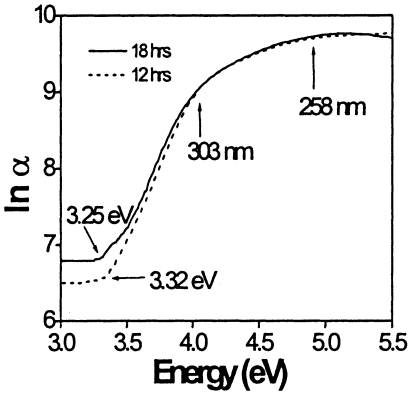


FIG. 6. Plot demonstrating the ln α versus energy (eV), which follows the Urbach's rule.

photocatalysis.[7,35] Inagaki et al. prepared anatase crystals with slightly larger crystallite size from $TiOSO_4$ to demonstrate the photocatalytic performance.[36] A solvothermal route is used to synthesize brookite powders.[37] In this report, photocatalysis was carried out on the anatase nanoparticles, simultaneously demonstrating oxidizing and reducing reactions. It is well known that potassium dichromate and formic acid are both toxic water pollutants. By a simple photocatalytic reaction in UV-visible region using $TiO_2$ as catalyst these pollutants could be simultaneously converted into their benign form as follows: Potassium dichromate is converted into chromium (III) hydroxide, which precipitates out, and formic acid is converted into carbon dioxide respectively.[38] In a typical reaction, potassium dichromate was used to prepare a 1 mM concentration of Cr(VI) solution and HCOOH concentration was adjusted at 0.0074 (M) to maintain the pH in the range 2.75–3, at which the dissociation of HCOOH into $HCOO^-$ and $H^+$ is most favorable.[39] Ten milliliters of the solution were taken in a small beaker to which 10 mg anatase $TiO_2$ was added, and the suspension was stirred continuously with magnetic stirrer for 30 min to enable Cr(VI) and HCOOH adsorption to reach an equilibrium before exposure of the mixture to the UV radiation. The above procedures were carried out at room temperature. The suspension was then placed under an UV source radiation ($\lambda = 365$ nm, power ~200 W) with constant stirring. After irradiation, the suspension was filtered, and the concentration of Cr(VI) and HCOOH in the reaction mixture was estimated by UV absorption and titration respectively.

## H. Mechanism

In aqueous medium, potassium dichronate undergoes complete dissociation. At pH ~2, the chromate ions remain as unprotonated $Cr_2O_7^{-2}$ and formic acid were ionized to formate ions. Complete adsorption of both ions takes place onto hydrated $TiO_2$ sites, denoted by an asterisk (*). In the presence of UV light, photo generation of electrons ($e^-_{cb}$) and holes ($h_{vb}^+$) results from $TiO_2$. These generated electrons and holes are responsible for the reduction of adsorbed $Cr_2O_7^{2-}$ and oxidation of adsorbed $HCOO^-$ ions, respectively. Equation 8 in Scheme 1 below shows the efficient prevention of electron-hole recombination.

The following is the scheme of elementary reactions proposed to explain the mechanism of photoreduction of Cr(VI).

$$K_2Cr_2O_7 \rightleftharpoons 2K^+ + Cr_2O_7^{-2} \quad (1)$$

$$HCOOH \rightleftharpoons HCOO^- + H^+ \quad (2)$$

$$Cr_2O_7^{2-} + 2TiO_2 \rightleftharpoons Cr_2O_7^{-2(2*)} \quad (3)$$

$$HCOO^- \rightleftharpoons HCOO^{-*} \quad (4)$$

$$TiO_2 \xrightarrow{h\nu} e^-_{cb} + h_{vb}^+ \quad (5)$$

$$Cr_2O_7^{-2(2*)} + 14H^+ + 6e^-_{cb} \rightarrow Cr(III)^* + 7H_2O \quad (6)$$

$$HCOO^{-*} + 2h_{vb}^+ \rightarrow CO_2 + H^+ + * \quad (7)$$

$$e^-_{cb} + h_{vb}^+ \rightarrow TiO_2 + \text{heat} \quad (8)$$

The present reaction sequence demonstrates the simultaneous oxidation and reduction of the reactants involved. Balancing the electrons and holes generated in Eqs. 6 and 7 results in 3 mol $HCOO^-$ ions being oxidized when 1 mol Cr(VI) ions is reduced. Starting with 1 mM concentration of potassium dichromate, 1 h UV exposure reduces this concentration to 0.678 mM. Two hours of exposure result in a residual concentration of 0.62 mM and this reduces with further exposure to UV radiation, becoming almost negligible after 3 h, indicating a complete consumption of the dichromate. It is emphasized that the concentration is below the detection limit of UV absorption. The UV absorption spectrum representing the change in concentration of the dichromate ions is shown in Fig. 7. UV absorption peak around 350 nm gradually

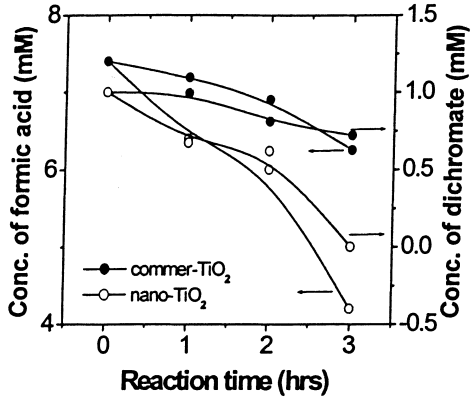


FIG. 7. Graph showing the amount of Cr(VI) reduced and formate oxidized with time. Comparison is made between the commercial powder and our nanoparticles.

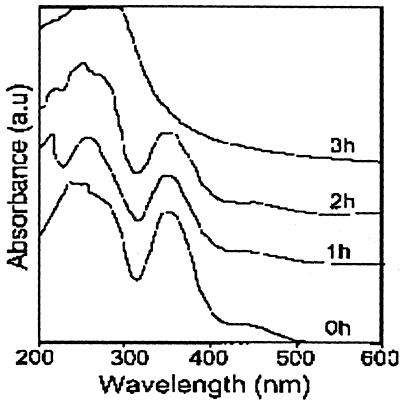


FIG. 8. UV absorption spectrum showing the reduction of Cr(VI) ion. The spectra are recorded for every 1 h of reaction.

diminishes with increase in time. Simultaneously, the formic acid consumption is indicated by the concentration that reduces from the initial 0.0074 to 0.0042 M in the same time period. A similar experiment was carried out using commercial $TiO_2$. Figure 8 shows the change of concentration of the reactants potassium dichromate and formic acid. This unambiguously demonstrates that the synthesized titania is superior in its photochemical activity compared to the commercial one.

## IV. CONCLUSIONS

Merely controlling the reaction conditions during the hydrothermal synthesis from titanium tetrachloride can result in single or mixed phases of highly crystalline titania without any additives. Pure anatase titania with particle size around 5–15 nm was obtained at 120 °C. Pure rutile titania with particle size around 15–25 nm was obtained at 250 °C. The photochemical efficiency of the synthesized anatase titania was tested and compared with that for commercial titania using a simple reaction whereby a simultaneous photochemical reaction converts pollutants like Cr(VI) and formate to non-pollutants like Cr(III) and carbon dioxide.

## ACKNOWLEDGMENTS

The authors are thankful to Department of Science & Technology, New Delhi for the financial support, and K.M.R. is thankful to Council of Scientific and Industrial Research, New Delhi for providing the Senior Research Fellowship. Our very special acknowledgements are due to late Prof. G.N. Subbanna, Head-MRC, Indian Institute of Science, India, for his invaluable help in recording TEM and electron diffraction patterns.

## REFERENCES

1. B. O'Regan and M. Grätzel: A low-cost, high efficiency solar cell based upon dye-sensitized colloidal $TiO_2$ films. *Nature* **353,** 737 (1991).
2. C.L. Perkins and M.A. Henderson: Photodesorption and trapping of molecular oxygen at the $TiO_2$(110)-water ice interface. *J. Phys. Chem. B* **105,** 3856 (2001).
3. Y.C. Yen, T.T. Tseug, and D.A. Chang: Electrical properties of porous titania ceramic humidity sensor. *J. Am. Ceram. Soc.* **72,** 1472 (1989).
4. T. Matsumoto, Y. Murakami and Y. Takasu: Photochromism of titanium oxide gels prepared by the salt-catalytic sol-gel process. *Chem. Lett.* **49,** 348 (2000).
5. R. Asahi, T. Morikawa, T. Ohwaki, K. Aoki, and Y. Taga: Visible light photocatalysis in nitrogen doped titanium oxides. *Science* **293,** 269 (2001).
6. A. Chemseddine and H.P. Boehm: A study of the primary step in the photochemical degradation of acetic acid and chloroacetic acids on a $TiO_2$ photocatalyst. *J. Mol. Catal.* **60,** 295 (1990).
7. J. Ovenstone and K. Yanagisawa: Hydrothermal synthesis and characterization of strontium doped lanthanum manganite perovskite powders for use as a cathode material in SOFCs. *Chem. Mater.* **11,** 2770 (1999).
8. E.S. Thiele and R.H. French: Light scattering properties of representative, morphological rutile titania nanoparticles using a finite element method. *J. Am. Ceram. Soc.* **81**[3], 469 (1998).
9. T.C. Patton: *Pigment Handbook* (Wiley, New York, 1973).
10. S.T. Aruna, S. Tirosh, and A.J. Zaban: Nanosize rutile particle synthesis via hydrothermal method without mineralizers. *J. Mater. Chem.* **10,** 2388 (2000).
11. L.H. Edelson and A.M. Glaeser: Role of particle substructure in the sintering of monosized titania. *J. Am. Ceram. Soc.* **71**[4], 225 (1988).
12. A. Chemseddine and T. Mritz: Nanostructuring titania: Control over nanocrystal structure, size, shape, and organization. *Eur. J. Inorg. Chem.* **2,** 235 (1999).
13. D. Zhang, L. Gao, and J. Guo: Effects of calcination on the photocatalytic properties of nanosized $TiO_2$ powders prepared by $TiCl_4$ hydrolysis. *Applied Catal., B: Gen.* **26,** 207 (2000).
14. H. Cheng, J. Ma, Z. Zhao, and L. Qi: Hydrothermal preparation of uniform nanosized rutile and anatase particles. *Chem. Mater.* **7,** 663 (1995).
15. C.C. Wang and J.Y. Ying: Sol-gel synthesis and hydrothermal processing of anatase and rutile titania nanocrystals. *Chem. Mater.* **11,** 3113 (1999).
16. H. Yin, Y. Wada, T. Kitamura, S. Kambe, S. Murasawa, H. Mori, T. Sakata, and S. Yanagida: Hydrothermal synthesis of nanosized anatase and rutile $TiO_2$ using amorphous phase $TiO_2$. *J. Mater. Chem.* **11,** 1694 (2001).
17. H. Kominami, J. Kato, S. Murakami, Y. Kera, M. Inoue, and B. Ohtani: Synthesis of titanium(IV) oxide of ultra-high photocatalytic activity: High-temperature hydrolysis of titanium alkoxides with water liberated homogeneously from solvent alcohols. *J. Mol. Catal. A* **144,** 165 (1999).
18. F. Cavani, E. Foresti, F. Parrinello, and F. Triro: Role of the chemistry of solutions of titanium ions in determining the structure of V/Ti/O catalysts. *Appl. Catal.* **38,** 311 (1998).
19. M. Henry, J.P. Jolivet, and J. Livage: In *Aqueous Chemistry of Metal Cations, Hydrolysis, Condensation and Complexation,* edited by R. Reisfeld and C.K. Jorgensen (Springer-Verlag, Berlin, Germany, 1992), p. 155.
20. L.I. Bekkerman, I.P. Dobrovolskii, and A. Ivakin: Effect of the composition of Ti(IV) solutions and precipitation conditions on the structure of the solid phase. *Russ. J. Inorg. Chem.* **21,** 233 (1976).
21. J. Livage, M. Henry, and C. Sanchez: Sol-gel chemistry of transition metal oxides. *Prog. Solid State Chem.* **18,** 259 (1988).
22. H.P. Klug and L.E. Alexander: In *X-ray Diffraction Procedures* (Wiley-Interscience, New York, 1974), p. 364.
23. R.A. Spurr and H. Myers: Quantity analysis of anatase-rutile mixture with an x-ray diffractomter. *Anal. Chem.* **29,** 760 (1957).

24. N.G. Park, G. Schlichthorl, J. van de Lagemaat, H.M. Cheong, A. Mascarenhas, and A.J. Frank: Dye sensitized $TiO_2$ solar cells: Structural and photochemical characterization of nanocrystalline electrodes formed from hydrolysis of $TiCl_4$. *J. Phys. Chem.* **103,** 3308 (1999).
25. T.M.J. Nilsson and G.A. Niklasson: Condensation of $H_2O$ by radiative cooling. *Sol. Energy Mater. Sol. Cells* **37,** 93 (1995).
26. C. Granqvist and T. Eviksson: in *Materials for Radiative Cooling to Low Temperatures,* edited by C. Granqvist (Pergamon Press, Oxford, U.K., 1991), p. 168.
27. K.N.P. Kumar, K. Keizer, A.J. Burggraaf, T. Okubo, and H. Nagamoto: Synthesis and textural properties of unsupported and supported rutile ($TiO_2$) membranes. *J. Mater. Chem.* **3,** 923 (1993).
28. S. Ardizzone, C.L. Bianchi, and B. Vercelli: Structural and morphological features of MgO powders: The key role of the preparative starting compound. *J. Mater. Res.* **13,** 2218 (1998).
29. S. Tsunekawa, T. Fukuda, and A. Kasuya: Blue shift in ultraviolet absorption spectra of monodisperse $CeO_{2-x}$ nanoparticles. *J. Appl. Phys.* **87,** 1318 (2000).
30. K. Madhusudan Reddy, S.V. Manorama, and A. Ramachandra Reddy: Bandgap studies on anatase titanium dioxide nanoparticles. *Mater. Chem. Phys.* **78,** 239 (2002).
31. Y.W. Zhang, R. Si, C.S. Liao, C.H. Yan, C.X. Xian, and Y. Kou: Facile alcohothermal synthesis, size-dependent ultraviolet absorption and enhanced CO conversion activity of ceria nanocrystals. *J. Phys. Chem. B* **107,** 10159 (2003).
32. Z. Yuhong, W. Ming, X. Gouxing, and Y. Weishen: Preparation and spectroscopic characterization of quantum size titanium dioixde. *Chin. J. Internet* **2,** 17 (2000).
33. B. Ullrich, D.M. Bagnall, H. Sakai, and Y. Segawa: Photoluminescence properties of thin CdS films on glass formed by laser ablation. *Solid State Commun.* **109,** 757 (1999).
34. M. Hirano, C. Nakahara, O. Tanaike, and M. Ingaki: Photoactivity and phase stability of $ZrO_2$-doped anatase-type $TiO_2$ directly formed as nanometer-sized particles by hydrolysis under hydrothermal conditions. *J. Solid State Chem.* **170,** 39 (2003).
35. J. Ovenstone: Preparation of novel titania photocatalysts with high activity. *J. Mater. Sci.* **36,** 1325 (2001).
36. M. Inagaki, Y. Nakazawa, M. Hirano, Y. Kobayashi, and M. Toyoda: Preparation of stable anatase-type $TiO_2$ and its photocatalytic performance. *Int. J. Inorg. Mater.* **3,** 809 (2001).
37. H. Kominami, Y. Ishii, M. Kohno, S. Konishi, Y. Kera, and B. Ohtani: Nanocrystalline brookite-type titanium(IV) oxide photocatalysts prepared by a solvothermal method: Correlation between their physical properties and photocatalytic activities. *Catal. Lett.* **91,** 41 (2003).
38. T.T.Y. Tan, D. Beydoun, and R. Amal: Photocatalytic reduction of Se(VI) in aqueous solutions in $TiO_2$ system:kinetic modelling and reaction mechanism. *J. Phys. Chem. B* **107,** 4296 (2003).
39. R. Chang: *Chemistry*, 5th ed. (McGraw-Hill, New York, 1994).